Stretching Servo Performances on a Spin Stand

Lu Feng, WaiEe Wong, Chunling Du, Chang Duan, Guo Xiao Guo, Tow Chong Chong, and Weichun Ye

Abstract— **To support a higher track recording density for future generation magnetic recording systems on a conventional spin stand, good servo controllers and high-bandwidth actuators are needed. In this work, we add an additional sub-stage piezo actuator with sub-nm resolution to an existing spin stand system. The combination of a frequency-encoded servo pattern and a simplified decoding scheme is applied to generate the position error signal (PES) by means of an external PC-based servo system. Various servo control techniques, namely, PID control, near-perfect modeling (NPM) low-hump design, low hump H_∞ control and feed-forward RRO compensation are designed and implemented on the same platform. Control performance comparison is then made and the experimental results show that PES 3σ is improved by up to 23.7% with the low-hump design together with the feedforward RRO compensation.**

I. Introduction

Spin stands or disk head testers are often used for high-speed electrical testing of magnetic heads, media and recording channel in both engineering and manufacturing environment [5]. Thus the demand for better servo performance on spin stands increases for future generation magnetic recording systems. In order to achieve the recording areal density of 1 terabit per square inch (Tbpsi) [13], bit sizes in disk drives are decreasing rapidly. As bit sizes decrease, thermal stability, fly height, and data rate issue make changes in the bit aspect ratio desirable. This places a tight restriction on the positioning of the read/write head [1].

Various factors impose fundamental limitations on the viability of high-track-density positioning, for instance, the presence of disk and motor vibrations [11], and the dynamics of mechanical structures. Requirements to reject the vibrations with good servo performances generally dictate increases in the servo bandwidth and decreases in the sensitivity peak. A decent control scheme to such a sensitivity function is thus required so that the disturbance within the servo bandwidth can be suppressed by the servo loop and the amplification of the disturbance beyond the bandwidth, due to the "waterbed effect", can be reduced [2].

In this work, a high-speed piezo chip translator (PZT), as a positioner, is integrated [6] with the head cartridge of a Guzik spin stand [5]. A frequency-encoded servo pattern and a simplified DFT decoding (FESDFT) scheme are combined [3] and used to generate a real-time position error signal (PES), which is employed to implement control strategies. Some different control techniques, namely, proportional-integral-differential (PID) design, NPM low-hump design [9], H_∞ low-hump control [11] and feedforward compensation [12] are applied to the positioning system on the spin stand. Servo performances of the spin stand system with these different controls are evaluated and compared.

Authors are with Data Storage Institute (DSI), A*STAR, 5 Engineering Drive 1, Singapore 117608 (phone: 65-68747825; fax: 65-67772053; e-mail: Lu_Feng@dsi.a-star.edu.sg).

II. System Configuration

A Guzik spin stand S1701A [5] is used to test read/write heads and media capabilities. The spin stand system provides the ease of writing servo patterns of different frequencies on media and measuring various properties of read/write heads and media. Combined efforts in the mechanical structure and electronic system of the commercial spin stand are paid to support heads and media for high-track-density demonstration [4].

The conventional spin stand consists of a piezo actuator with a displacement range of 12-16.5 μm and a linear scale resolution of 0.5 nm [5]. To stretch its servo capabilities, the head cartridge is modified to integrate a high-speed micro-actuator with a displacement range of 5-6 μm and a resolution of 0.02 nm, as a positioning device to achieve a high precision track following system [6]. In this way, bandwidth limitation of the piezo actuator on the conventional spin stand can be relaxed.

In addition, a low cost PC-based system is set up as the external servo system, which allows fast deployment and flexibility of testing different servo concepts. A high feedback rate of 15 kHz can be attained from this 3 GHz PC-based setup under Linux platform [7] and a higher immunity to non-idealities in readback signals is achieved using FESDFT scheme for PES generation [3]. The overall PC-based external servo system is configured as in Fig. 1. Development of both the mechanical structure and the advanced servo controller can attain further improvements to the performance of the existing spin stand system. In this case, we mainly focus on the advanced servo design.

A. PZT Micro-actuator Design

As PZT actuated suspensions attached with read/write heads are not available for testing on the spin stand, alternatively a low voltage piezo translator chip (LVPZT)

of 3 mm by 3 mm dimension is used to provide precise positioning of the read/write heads. The Guzik head cartridge is modified and the PZT is inserted within a small gap to provide a sub-nanometer movement for servo control. This designed micro actuator can also be used to test sliders while the PZT actuated suspension cannot. In order to move the head with a sufficiently high servo bandwidth, the PZT micro-actuator is required to have a high resonant frequency. Details on the PZT head cartridge modification can be seen in [6].

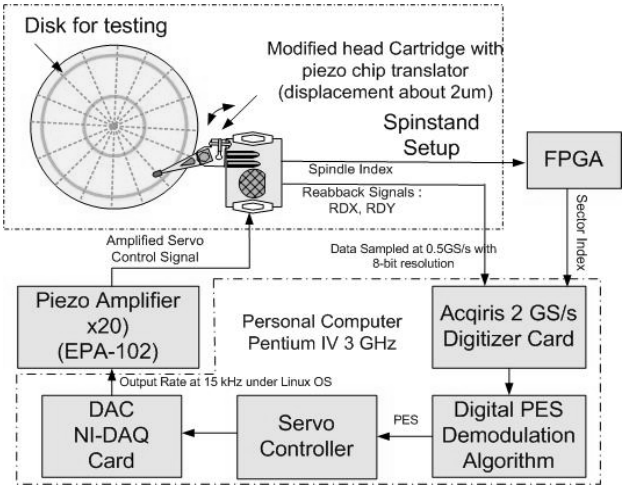

Fig. 1. Block diagram of system configuration.

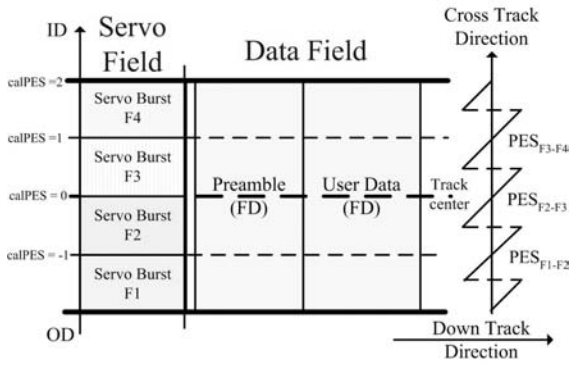

Fig. 2. Frequency-encoded servo pattern layout.

B. PES Calculation

Due to the limited displacement of the PZT actuator, servo patterns of four different frequencies, 31.25 MHz, 25 MHz, 20 MHz and 12.5 MHz are written on the 2.5" magnetic disk to represent four servo tracks of 9 μinch and the layout is shown as in Fig. 2. DFT components of individual servo track are extracted to form the individual PES_{servo}. These individual DFT components of the servo pattern are calibrated and combined to form a suitable position error signal as in Fig. 3. More details on PES calculation are given in [3].

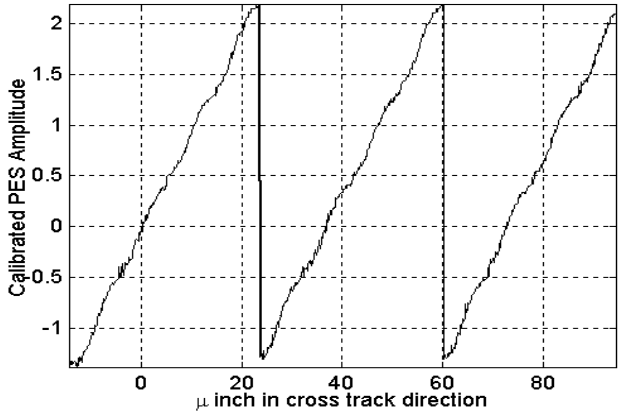

Fig. 3. Calibrated PES where 1 unit corresponds to the servo track width.

The processing of the position error signal is performed on the digitized read back signal from the pre-amplified transducer. The position error signal is then demodulated on a real-time system and ready to be fed to the servo controller for thermal drift elimination and track following operation.

C. Modeling of the Modified PZT Head Cartridge

The plant can be subdivided into three components: the PZT translator chip, the head cartridge base and the non-active suspension with the read/write head. The frequency response of the plant measured by calculated PES is shown in Fig. 4, where the smooth curve is from the identified model:

$$P(s) = \frac{-2.122\times10^{9}(s-1.235\times10^{4})(s^{2}+2477s+2.104\times10^{9})}{(s+1.235\times10^{4})(s^{2}+3458s+7.3\times10^{8})(s^{2}+2325s+2.162\times10^{9})}$$

It should be noted that after the modification, the frequency of the dominant resonance is pushed up to 4.3 kHz.

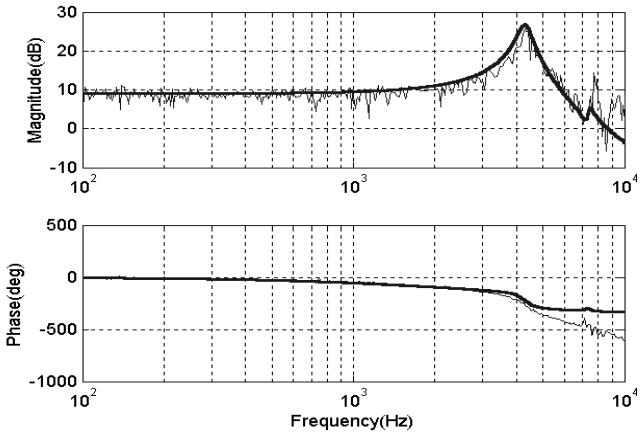

Fig. 4. PZT micro actuator with the modified head cartridge.

III. Servo Control Design

A good servo system needs a high control bandwidth to attain sufficient positioning accuracy by suppressing the effect of various disturbances. The sampling frequency limits the bandwidth due to loss of phase margin. Digital controller poles and zeros cannot be set higher than the Nyquist frequency, i.e., half of the sampling frequency, and the dynamics that are above the Nyquist frequency may cause problems due to aliasing [9]. In our real-time spin stand system, the sampling frequency can reach 15 kHz based on the developed calculation method of digital PES in spite of the hardware limits. This section presents the details of four control schemes: PID, NPM low-hump, H_∞ low-hump and feedforward compensation.

A. PID Control Design

PID algorithm is applied to this spin stand system. Fig. 5 gives the simplified block diagram of the read servo control system. PID controller $C(s)$ is designed in continuous time domain and converted to discrete form

$$C(z) = k_p + k_d \frac{2}{T_s} \cdot \frac{z-1}{z+1} + \frac{k_i}{\frac{2}{T_s} \cdot \frac{z-1}{z+1} + 10} \quad (1)$$

with PID parameters k_p, k_d, k_i and sampling time T_s, using bilinear transformation.

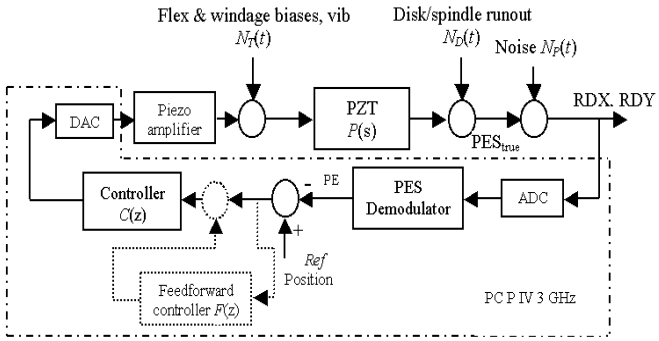

Fig. 5. Block diagram of the servo control system.

A servo bandwidth of 1020 Hz is obtained with the PID controller with k_p = 0.12, k_i = 2400, and k_d = 0 and a notch filter, shown as in Fig. 6. The measured frequency responses of the closed-loop $C(z)P(z)/(1+C(z)P(z))$ and sensitivity function $1/(1+C(z)P(z))$ are shown as in Fig. 7, where we can see the peak value of the sensitivity function is 6.5 dB.

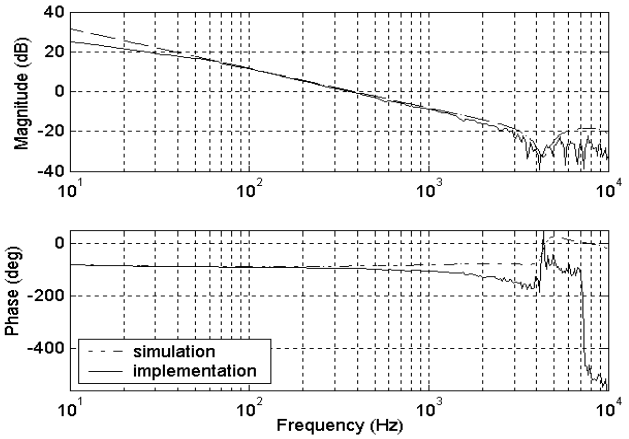

Fig. 6. Frequency response of the controller.

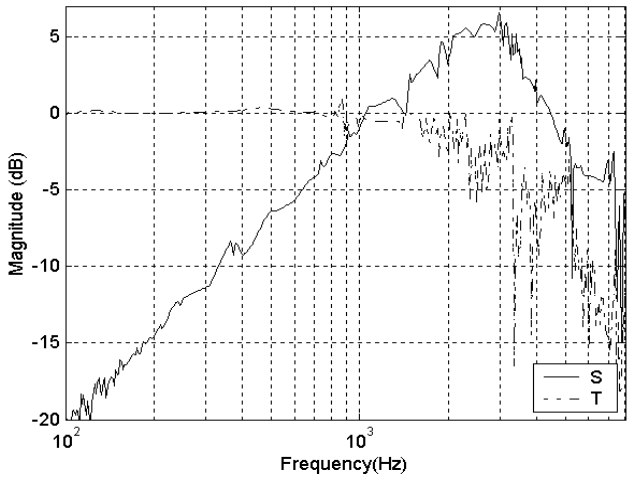

Fig. 7. Sensitivity and closed-loop functions with the PID control.

B. NPM Low-hump Control Design [9]

In addition to the open loop frequency response, which determines the bandwidth and stability margins, another important frequency response is that of the sensitivity function. One of the servo design objectives is to make the magnitude of sensitivity functions small, so that the disturbances within the servo bandwidth can be suppressed, while the amplification to disturbances beyond the bandwidth due to the sensitivity hump can be remained least. According to Bode's Integral Theorem [14], for stable plant P and controller C with $P(s)C(s)$ of at least 2-pole roll off, the integral of the log magnitude of the sensitivity function over frequency from zero to infinity must equal to zero. Moreover, the sensitivity function has a higher amplitude peak for discrete-time systems, compared to continuous-time systems with similar low-frequency characteristics and bandwidth. The peak will be increasing if the sampling frequency is being decreased [2].

Conventional notch filter-based servo which compensates the resonant poles in the plant model alone is insufficient as the loop gain at the frequencies of the anti-resonant zeros are very small, and hence causing a hump in the sensitivity function at these frequencies. As such, the anti-resonant zeros should be compensated as well to achieve a low-lump sensitivity for better disturbance rejection.

The so-called NPM [9] of micro-actuators is to construct a virtual model that has a flat magnitude up to a frequency as high as possible. Such model is composed of the real micro-actuator plant and a model inverse which compensates both resonant poles and anti-resonant zeros of

the micro-actuator model.

The PZT micro-actuator can be viewed as a pure unity gain up to a high frequency after pre-multiplying with model inverse from NPM. With the PID servo control associated with the model inverse, we can obtain a higher bandwidth and a lower sensitivity hump as in Fig. 10, where the peak value of the sensitivity hump is reduced to 4.5 dB with 1050 Hz servo bandwidth. Fig. 8 and 9 show, respectively, the frequency responses of the designed controller and the compensated open loop.

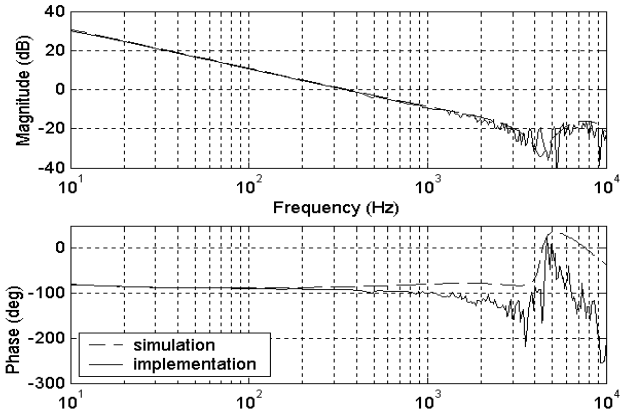

Fig. 8. Frequency response of the controller.

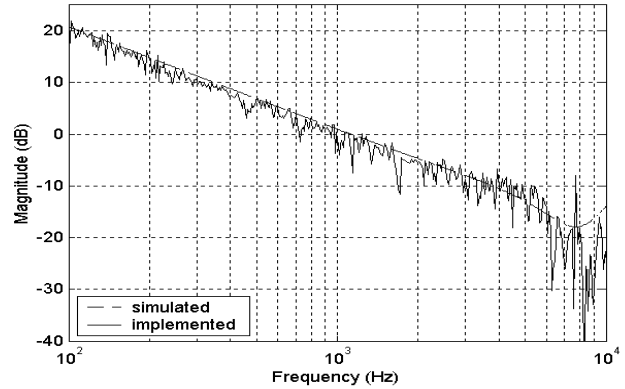

Fig. 9. Open loop frequency response.

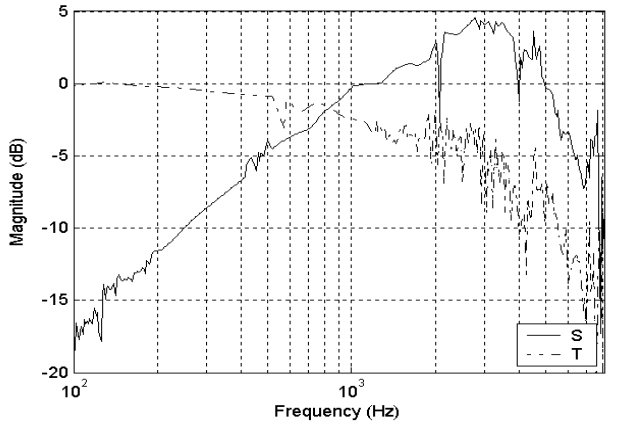

Fig. 10. Sensitivity and closed-loop functions with the low-hump design.

C. Low-order H_∞ Loop Shaping with Low-hump Sensitivities

Another control technique to reduce the sensitivity hump is based on H_∞ loop shaping method. Specifications for the control system performance are prescribed as follows:

- Bandwidth of at least 900 Hz (i.e., sensitivity function 0 dB crossover frequency of at least 900 Hz).
- A sensitivity function peak of no more than 5 dB.
- At least 15 dB disturbance rejection at 100 Hz.

When the plant is augmented with weighting functions W_1, as in Fig. 11, the H_∞ controller can be obtained with the restriction of $\|W_1 S\|_\infty < 1$, where S is the sensitivity function (error rejection). Therefore, when W_1^{-1} is defined according to the prescribed specifications for the desired error rejection, the controller C can be obtained

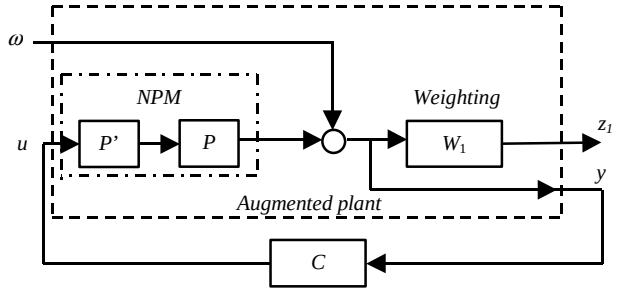

Fig. 11. Design method of the H_∞ loop shaping.

systematically. Here, we use a linear matrix inequality (LMI) approach [15] to design the controller with the H_∞ loop shaping method.

With the model inverse P', the plant model can be constructed into a simplified model NPM whose frequency response is a pure unity gain up to a high resonant frequency. The H_∞ loop shaping is carried out for the simplified model NPM and thus the ultimate controller is $C(z)\cdot P'(z)$, where $C(z)$ is designed by the H_∞ loop shaping method. Fig. 12 and 13 show the frequency responses of the designed controller and the compensated open loop. The frequency responses of the sensitivity and the closed-loop transfer functions are shown in Fig. 14, where the sensitivity 0 dB crossover frequency is 955 Hz and the sensitivity peak value is 4.5 dB.

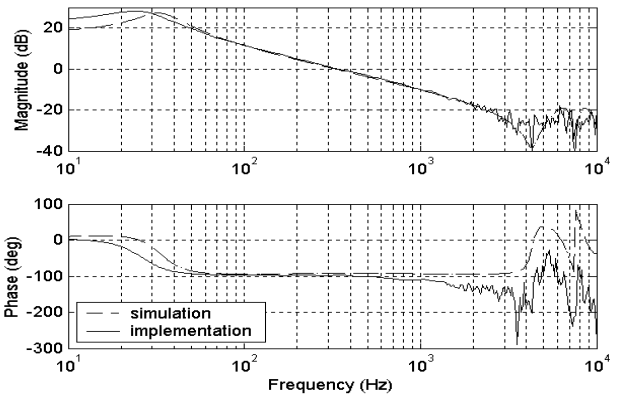

Fig. 12. Frequency response of the controller.

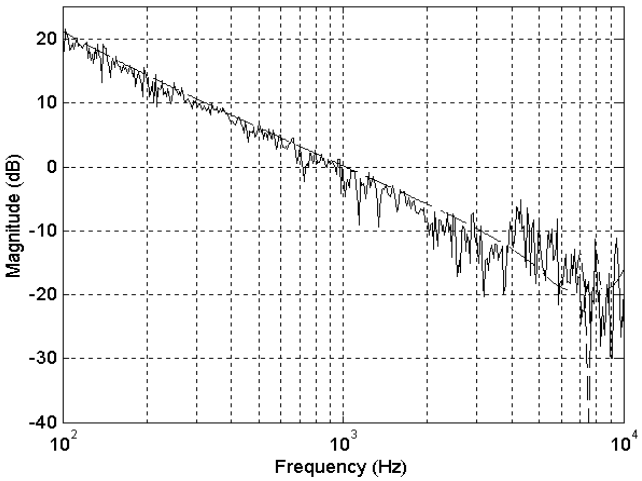

Fig. 13. Open loop frequency response.

D. Feedforward Compensator Design [12]

In this work, besides the earlier feedback controls, a feedforward compensator is designed to compensate RRO by the adaptive feedforward runout compensation (AFC) method [12]. The feedforward compensator $F(z)$ is given by

$$F(z) = \sum_i \frac{g_i z[z\cos(\phi_i) - \cos(\omega_i T_s + \phi_i)]}{z^2 - 2\cos(\omega_i T_s) z + 1} \qquad (2)$$

where ω_i are the selected RRO harmonics to be cancelled, g_i are the constant adaptation gains. As shown in Fig. 5, the system adopts "plug-in" configuration for realizing the feedforward compensation scheme.

IV. Implementation Results and Analysis

The developed controls in Section III were implemented on the spin stand with a motor rotational speed of 4000 rpm. Fig. 15a shows the PES spectrum comparison with the notch-filter-based PID control and without controls. Fig. 15b shows the comparison between the NPM low-hump control and the H_∞ low hump control. Fig. 15c shows the comparison with and without the feed-forward compensation under the NPM low-hump control. The comparison of PES σ values versus frequencies with the developed servo controls is shown in Fig. 16, where we can

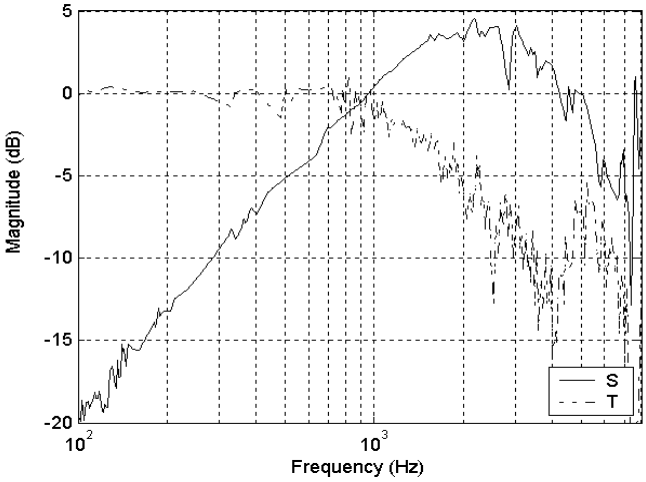

Fig. 14. Sensitivity and closed-loop functions with the H_∞ low-hump design.

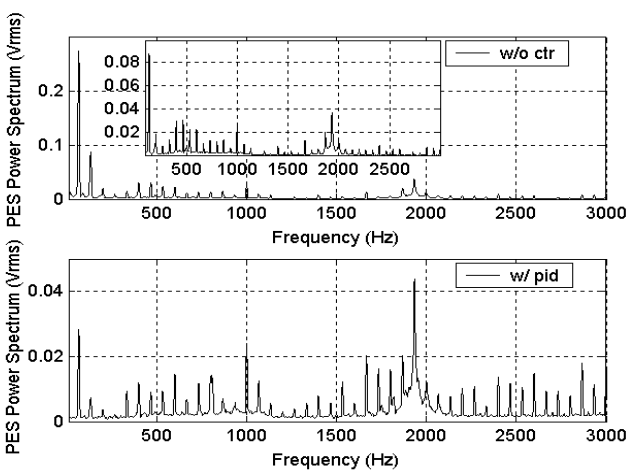

(a)

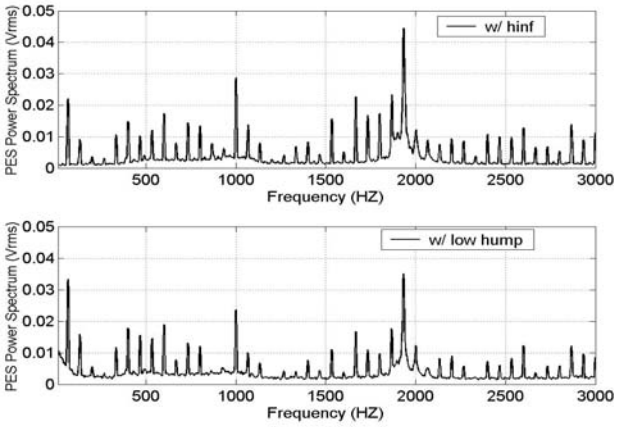

(b)

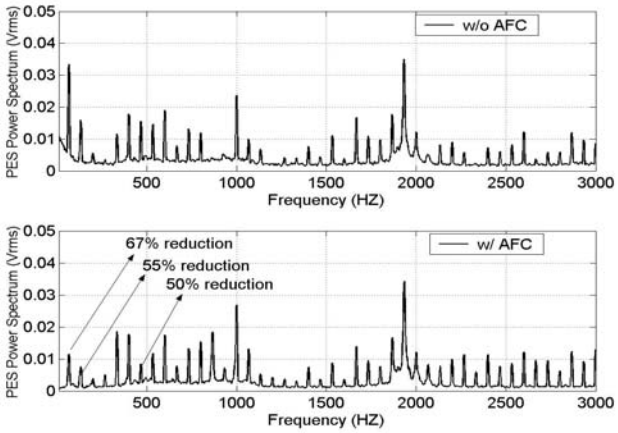

(c)

Fig.15. (a) PES spectra with and without PID control. (b) PES spectra with H_∞ low-hump and NPM low-hump designs. (c) PES spectrum comparison with and without feedforward control.

see the bottom curve, i.e., the smallest PES σ, is achieved with the low-hump design accompanied by the feedforward RRO compensation.

Table 1 summarizes the control performances achieved by the developed control schemes implemented on the spin stand system. The PES 3σ is reduced by 16% when the PID controller is used. With the low-hump controller activated, the PES 3σ value is reduced by 21.9%, which is better than that with the PID controller. The improvement is mainly attributed to the lower peak value of the sensitivity function and higher servo bandwidth. With the H_∞ control, the PES 3σ has reached a reduction of 16.7%. Using the feed-forward compensator, the PES 3σ is reduced by 23.7% with the cancellation of a few selected RRO components.

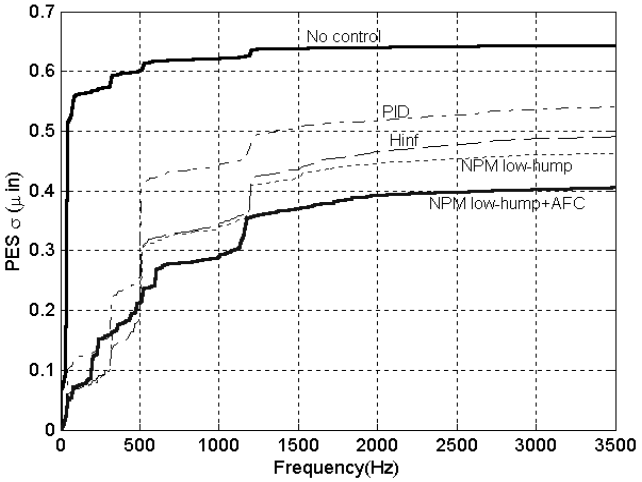

Fig. 16. PES σ value versus frequency.

Table 1. Servo performance comparison with different controls.

Methods\items	Bandwidth (Hz)	Sensitivity peak (dB)	PES 3σ (μinch)	Disturbance reduction (%)
W/o contr.	-	-	2.01	-
PID	1020	6.5	1.688	16
H_∞ Low-hump	955	4.5	1.6738	16.7
NPM Low-hump	1050	4.5	1.5708	21.9
NPM Low-hump + AFC	1050	4.5	1.534	23.7

V. CONCLUSION

To achieve high servo performance under the limited sampling rate, some feedback controllers have been designed and implemented on the real-time spin stand with the help of an external PC-based servo control system. Adaptive feed-forward compensation method has also been employed to reject RRO caused by spindle motor. The servo performance comparison with different control schemes such as PID, NPM low-hump, H_∞ low-hump control and feedforward compensation has been made. The results have shown that the vibration rejection has been improved tremendously with the external servo control for the spin stand. Therefore using this flexible external servo control system, the current spin stand can continue to be used for testing high-areal-density heads and media.

REFERENCES

[1] D. Abramovitch and G. Franklin, "A brief history of disk drive control," *IEEE Control Systems Magazine, V*ol. 22, No. 3, pp.28-42, Jun. 2002.

[2] Matthew T. White and Wei-Min Lu, "Hard disk drive bandwidth limitations due to sampling frequency and computational delay," *Proc. of 1999 IEEE/ASME International Conference on Advanced Intelligent Mechanics*, pp. 120-125, Sep. 19-23, 1999.

[3] W. E. Wong, L. Feng, G. Guo, W. Ye, and A. Al-Mamun, "Implementation of a servo positioning system on spin stand," *Proc of 29th Annual Conf. of the IEEE Industrial Electronics Society, IECON*, pp. 2114-2119, Nov. 2003.

[4] Z. Zhang, Y. C. Feng; T. Clinton, G. Badran, N. H. Yeh, E. Girt, S. Harkness, M. Munteanu, H. J. Richter, R. Ranjan, S. Hwang, G. C. Rauch, M. Ghaly, D. Larson, E. Singleton, V. Vas'ko, J. Ho, F. Stageberg, V. Kong, K. Duxstad, and S. Slade, "Magnetic recording demonstration over 100~Gb/in^2," *IEEE Trans. Magn.*, 38(5), pp. 1861-1866, Sep. 2002.

[5] Guzik Company Website [online], Spin Stand Products Information, **http://www.guzik.com/**.

[6] Z. He, G. Guo, L. Feng, and W.E. Wong, ``Design of a head carrying~cartridge with micro actuation for high density magnetic recording," *2nd Int. Conf. on Computational Intelligence, Robotics and Autonomous Systems, CIRAS*, Dec. 15-18 2003.

[7] J. Liu, W.E. Wong, L. Feng, and G. Guo, "Implementation of a high performance multirate control system using PC," *Proc. of IEEE Int. Conf. on Power Electronics and Drive Systems*, PEDS, pp. 636 –641, Nov. 17-20 2003.

[8] Physik Instrumente (PI) Company Website [Online], Piezo Products Information, http://www.physikinstrumente.com.

[9] C. K. Pang, D. Wu, G. Guo, T.C. Chong, and Y. Wang, "Suppressing sensitivity hump in HDD dual-stage servo systems," *Proc. 2003 JSME-IIP/ASME-ISPS Joint Conf. Micromechatronics for Information & Precision Equipment* (IIP/ISPS Joint MIPE'03), pp. 26-27, Yokahama, Japan, June 16-18, 2003.

[10] R. Chen, G. Guo, T. Huang, and T. S. Low, "Optimal multirate control design for hard disk servo systems," *IEEE Trans Magn*, pp. 1898-1990, July 1998.

[11] C. Du, J. Zhang, and G. Guo, "Vibration analysis and control design comparison of HDDs using fluid bearing and ball bearing spindles," *Proc. of 2002 American Control Conf.*, pp. 1378-1382, May 2002.

[12] J. Zhang, R. Chen, G. Guo**,** and T. S. Low, "Modified adaptive feedforward runout compensation for dual stage servo system," *IEEE Trans. on Magnetics*, 36(5), Part: 1, pp. 3581-3584, 2000.

[13] R. W. Wood**,** J. Miles, and T. Olson, "Recording technologies for terabit per square inch systems,**"** *IEEE Trans. on Magnetics*, 38(4), pp. 1711–1718, 2002.

[14] H. W. Bode, "Network analysis and feedback amplifier design," Van Nostrand, Princeton, 1945.

[15] C. Scherer, P. Gahinet, and M. Chilali, "Multiobjective output-feedback control via LMI optimization", *IEEE Trans. Automatic Control*, vol. 42, No. 7, pp. 896-911, 1997.